Observation of the magnetic flux and threedimensional structure of skyrmion lattices by electron holography

Hyun Soon Park^{1†}*, Xiuzhen Yu¹, Shinji Aizawa¹, Toshiaki Tanigaki¹, Tetsuya Akashi², Yoshio Takahashi², Tsuyoshi Matsuda³, Naoya Kanazawa⁴, Yoshinori Onose⁵, Daisuke Shindo^{1,6}, Akira Tonomura^{2‡} and Yoshinori Tokura^{1,4}

Skyrmions are nanoscale spin textures that are viewed as promising candidates as information carriers in future spintronic devices¹⁻³. Skyrmions have been observed using neutron scattering^{4,5} and microscopy techniques⁶⁻¹¹. Real-space imaging using electrons is a straightforward way to interpret spin configurations by detecting the phase shifts due to electromagnetic fields. Here, we report the first observation by electron holography of the magnetic flux and the three-dimensional spin configuration of a skyrmion lattice in Fe_{0.5}Co_{0.5}Si thin samples. The magnetic flux inside and outside a skyrmion was directly visualized and the handedness of the magnetic flux flow was found to be dependent on the direction of the applied magnetic field. The electron phase shifts φ in the helical and skyrmion phases were determined using samples with a stepped thickness t (from 55 nm to 510 nm), revealing a linear relationship ($\varphi = 0.00173t$). The phase measurements were used to estimate the three-dimensional structures of both the helical and skyrmion phases, demonstrating that electron holography is a useful tool for studying complex magnetic structures and for three-dimensional, real-space mapping of magnetic fields¹².

Topological spin textures have been attracting increasing interest for use in studying quantum magneto-transport and for possible applications in spintronics. Skyrmions are particularly attractive for use as information carriers in memory and logic devices because of the emergence of spin transfer torque at extremely low current densities ($\sim 1 \times 10^6 \text{ A m}^{-2}$)^{2,3,13,14}. A skyrmion carrying a topological quantum number acts as an effective magnetic flux. Charge carriers flowing over the skyrmion crystal are deflected by the emergent electromagnetic field induced by this magnetic flux, giving rise to the topological Hall effect^{15,16}. Several challenges must be addressed before the skyrmion can be applied to actual devices. These include the realization of skyrmions at room temperature, clarification of their three-dimensional structures, and the fabrication of thin films containing skyrmions. Despite recent theoretical studies¹⁷⁻¹⁹, the three-dimensional structures of skyrmions remain elusive. Observing the three-dimensional structures of skyrmions at the microscopic level is a prerequisite for applications of skyrmions to spin-electronic devices.

Real-space imaging of skyrmion lattices has been performed by using the Fresnel (out-of-focus) method of Lorentz electron

microscopy (LEM) in thin samples of metals, semiconductors and insulators^{6-8,20}. The Fresnel method has enabled the direct observation of the motions (dynamics) of vortices, domain walls and skyrmions spanning from the millisecond to the nanosecond regime^{14,21-24}. However, quantitative analysis of the magnetic flux flow inside and outside a skyrmion is quite difficult because of both the resolution limit (due to the defocused condition) and the unwanted artefacts (surface roughness or contamination) of thin samples.

A skyrmion lattice on the surface of bulk $Fe_{0.5}Co_{0.5}Si$ crystal was recently observed with a spatial resolution of $\sim\!20$ nm using magnetic force microscopy (MFM) 10 . Because MFM detects only the stray fields leaking from the sample surface, interpretation of magnetic flux in the vicinity of skyrmions is not straightforward. Furthermore, the magnetic state of the sample can be easily affected by the probe tip geometry and the surface condition of the sample.

Electron holography, using the wave nature of electrons, provides opportunities for directly detecting and visualizing, in real space, the phase shifts φ of electron waves due to electromagnetic fields²⁵. However, precise phase measurement of weak phase objects such as skyrmions is very challenging because procedures are needed to average the phase images and separate the electric and magnetic vector potentials. Nevertheless, the advantage of electron holography over LEM and MFM under the just-focused condition makes it possible to visualize a quantized magnetic flux with nanometre resolution, in addition to determining its density in the vicinity of skyrmions. We investigated the two-dimensional magnetic flux distributions of a skyrmion lattice in helimagnet Fe_{0.5}Co_{0.5}Si thin samples and estimated the three-dimensional structures of the helical and skyrmion phases using high-voltage holography electron microscopes.

Figure 1a presents an image of a thin sample produced by the focused ion beam (FIB) technique as well as its schematic design. The diffraction pattern in the inset to Fig. 1a shows the characteristics of the single crystal when the incident electron beam is parallel to the [001] (z) direction. The contrast (Fig. 1a) changes visibly along the sample as the sample thickness varies. The 510 nm thickness was at least five times larger than the helical period. The purpose of using samples with a stepped thickness was to clarify the three-dimensional structures of the helical and skyrmion phases in the z direction. We investigated whether φ in these phases is equal.

¹RIKEN Center for Emergent Matter Science (CEMS), 2-1 Hirosawa, Wako, Saitama 351-0198, Japan, ²Central Research Laboratory, Hitachi Ltd, 2520 Akanuma, Hatoyama-machi, Hiki-gun, Hatoyama, Saitama 350-0395, Japan, ³Japan Science and Technology Agency, 4-1-8, Honcho, Kawaguchi-shi, Saitama 332-0012, Japan, ⁴Department of Applied Physics and Quantum-Phase Electronics Center (QPEC), University of Tokyo, 7-3-1, Hongo, Bunkyo-ku, Tokyo 113-8656, Japan, ⁵Department of Basic Science, University of Tokyo, 3-8-1 Komaba, Meguro-ku, Tokyo 153-8902, Japan, ⁵Interdisciplinary Materials Research for Advanced Materials, Tohoku University, 1-1-2-chome, Katahira, Aoba-ku, Sendai 332-0012, Japan. †Present address: Department of Materials Science and Engineering, Dong-A University, Saha-gu, Busan 604-714, Republic of Korea. †Deceased. *e-mail: hspark@riken.jp; hsparkaem1@dau.ac.kr

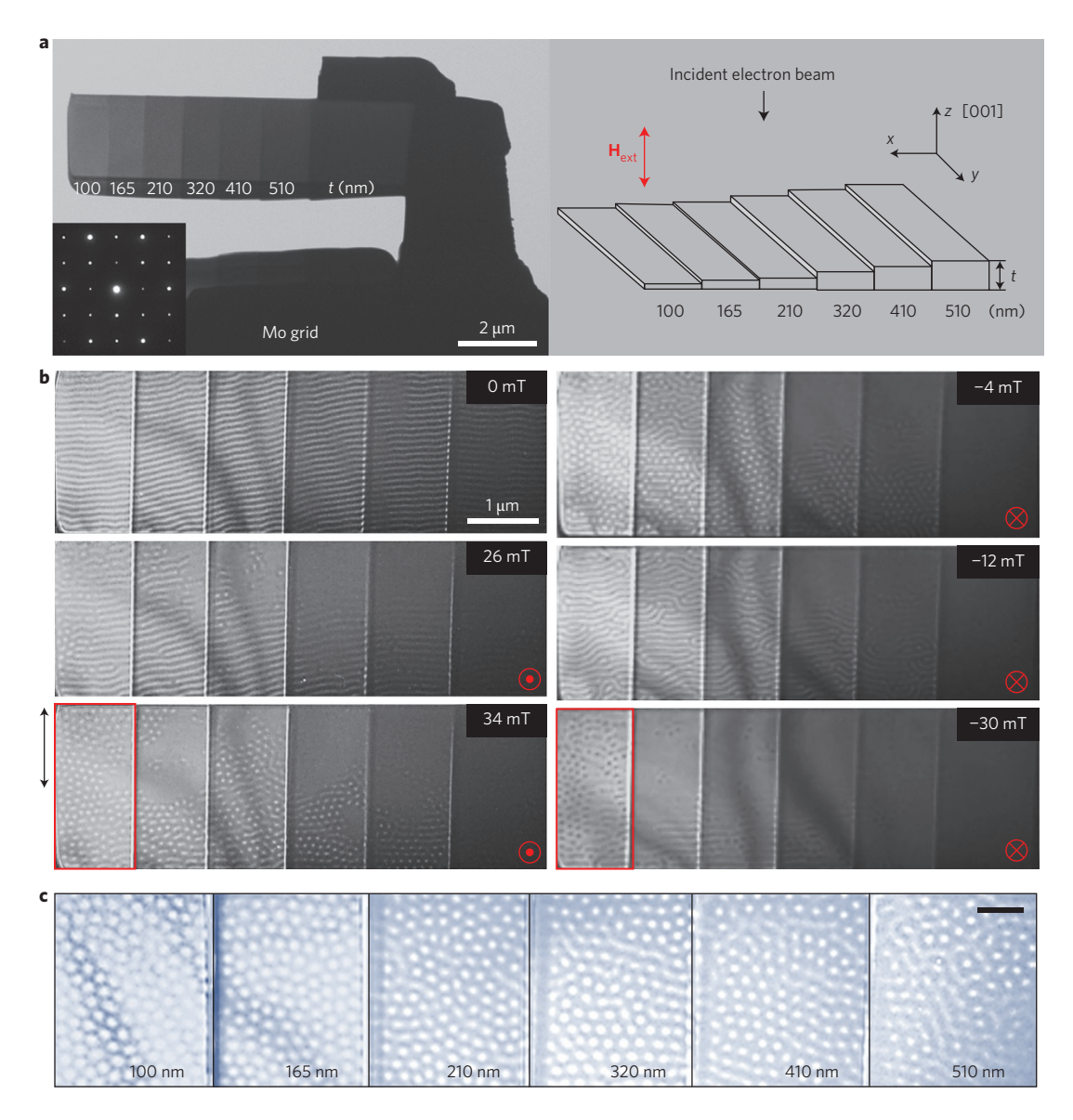


Figure 1 | Lorentz micrographs of an $Fe_{0.5}Co_{0.5}Si$ thin sample. a, Image and schematic illustration of a thin sample produced using the FIB technique. Thickness differences are represented as different levels of contrast. H_{ext} represents the applied field. Left inset: Diffraction pattern for electrons incident along the [001] zone axis. \mathbf{b} , Change in magnetic configuration with increase in field applied normal to the film (image) plane at T = 12 K. Applied fields are indicated in each image, and red symbols indicate the field direction. All images were taken in over-focused conditions (defocused value, \sim 1.4 mm) using the out-of-focus Fresnel method in Lorentz microscopy. The contrast reversal of the skyrmion lattice is clearly shown in the panels indicated by red rectangles. The black double-headed arrow indicates the sample edges corresponding to the area observed in \mathbf{c} . \mathbf{c} , Thickness dependence of skyrmion lattices along sample with field cooling at 25 mT and 12 K. Image contrast was independently adjusted for each image to clarify the skyrmion lattice. Scale bar, 300 nm.

Lorentz micrographs obtained using a 1,000 kV microscope (Fig. 1b,c) show the changes in magnetic structure as a function of the field applied normal to the film plane at $T\!=\!12\,\rm K$. Note that the local temperature of thin samples may vary due to the sample geometry. Stripe domains, shown as bright and dark lines in Fig. 1b, are clearly visible over the entire sample with zero-field cooling. The direction of the domains was observed to be parallel to the [100] direction, and the helical period was estimated to be $\sim\!90$ nm and independent of sample thickness.

When a magnetic field of 26 mT was applied, some stripes changed into white dots, forming a skyrmion lattice. The dots were located mainly near the edges of the areas with thicknesses of 100, 165 and 210 nm. At 34 mT, a skyrmion lattice was observed over the entire sample and the size of the dots decreased with increasing thickness. A skyrmion lattice was not observed near sample edges that were more than 300 nm thick.

Interestingly, when a field of $-4\,\mathrm{mT}$ was applied, the white dot domains remained. Eventually, the skyrmion lattice of white dots changed to black dots when the field reached $-30\,\mathrm{mT}$ (red rectangle in Fig. 1b). Note that, with field cooling (25 mT, 12 K, Fig. 1c), a skyrmion lattice was observed even near the sample edges corresponding to the area indicated by the black double-headed arrow at $34\,\mathrm{mT}$.

We now turn to the visualization of the magnetic flux in the vicinity of the skyrmion lattice using electron holography. In offaxis electron holography, in which one wave passes through a vacuum and the other through the specimen, the phase difference can be obtained from the hologram. The closed path made by the two paths can be assumed to lie in the x-z plane (Fig. 5c). For a thin film of thickness t and in-plane magnetization (in the y direction), in the case where the leakage of the field into the vacuum is negligible, the phase change $\Delta \varphi$ is expressed as

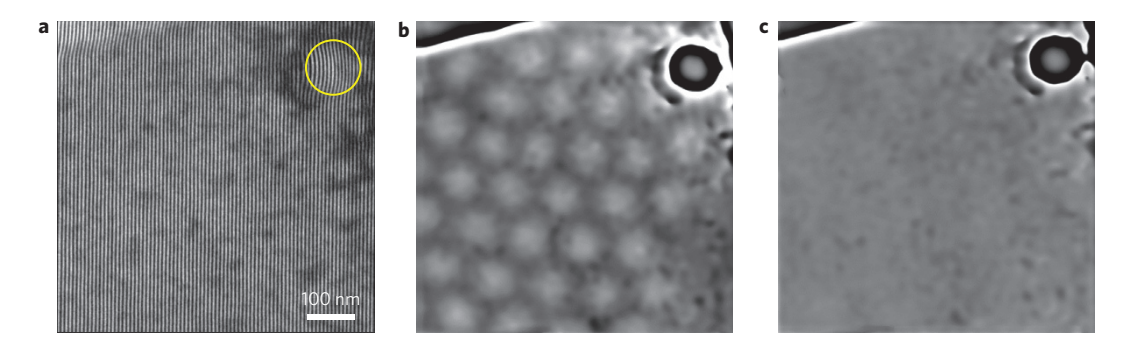


Figure 2 | Phase maps showing the skyrmion lattice and paramagnetic state. a, Hologram of the skyrmion lattice at 25 mT and T = 10.6 K. The yellow circle indicates a hole created by the FIB technique to facilitate alignment of 64 phase images. b, Phase image reconstructed from the hologram in a (T = 10.6 K, below the Curie transition temperature T_c), showing phase shifts due to both electric (φ_E) and magnetic (φ_M) vector potentials of the skyrmion lattice. c, Phase image of the paramagnetic state obtained at 25 mT and T = 41.6 K (above T_c), showing φ_E only.

$$\Delta \varphi = C_{\rm E} V_0(x, y) t(x, y) - \frac{2\pi e}{h} \iint B_{\rm n}(x, y) \mathrm{d}x \mathrm{d}z \tag{1}$$

where $C_{\rm E}$ is the interaction constant (0.00652 rad V⁻¹ nm⁻¹ for 300 keV electrons and 0.00538 rad V⁻¹ nm⁻¹ for 1,000 keV electrons), $V_0(x, y)$ is the projected mean inner potential, t(x, y) is the

projected thickness, h is Planck's constant, e is the elementary electric charge, and $B_{\rm n}$ is the component of the magnetic field normal to the plane defined by the beam paths, that is, in the y direction. Details of the electron holography method can be found elsewhere^{25–27}.

Figure 2a presents a hologram (interference fringes) taken at T = 10.6 K and 25 mT. It was formed using an electron biprism

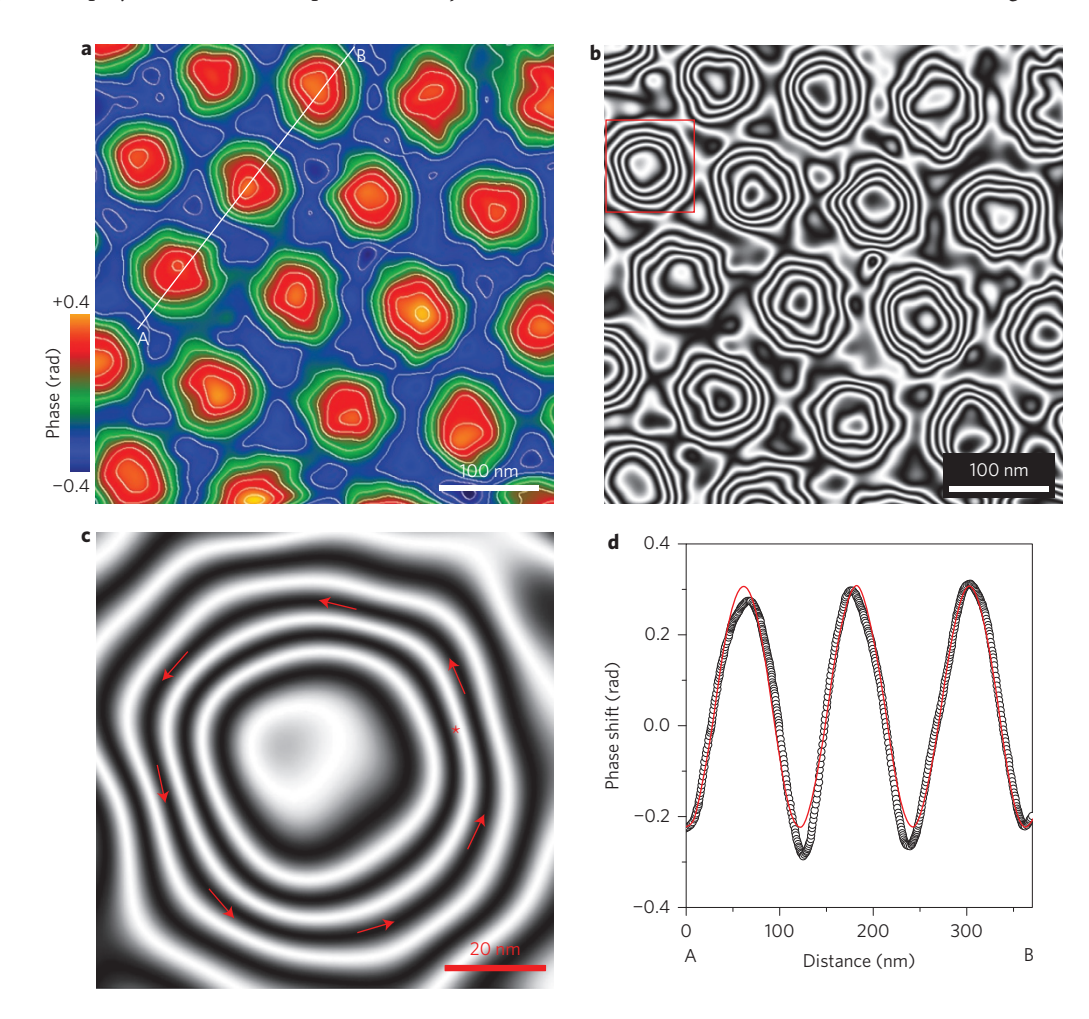


Figure 3 | Magnetic flux maps of the skyrmion lattice. $\bf a$, Two-dimensional map showing the phase shift due to magnetic vector potential φ_M . The difference between equi-phase lines corresponds to 0.1 rad. A plot along A-B is shown in $\bf d$. $\bf b$, Magnetic flux flow in the skyrmion lattice. Black and white lines correspond to lines of magnetic flux. $\bf c$, Enlarged image corresponding to the area indicated by the red square in $\bf b$. Red arrows indicate direction of lines of magnetic flux (anticlockwise). The phase difference between black contours corresponds to $\pi/25$. The asterisk in red indicates the region in which we determined the in-plane component of the magnetic flux density. $\bf d$, Phase shift profile corresponding to line A-B in $\bf a$. A fit to the sinusoidal waveform is shown in red. The measured period of the skyrmion lattice is 120.8 nm.

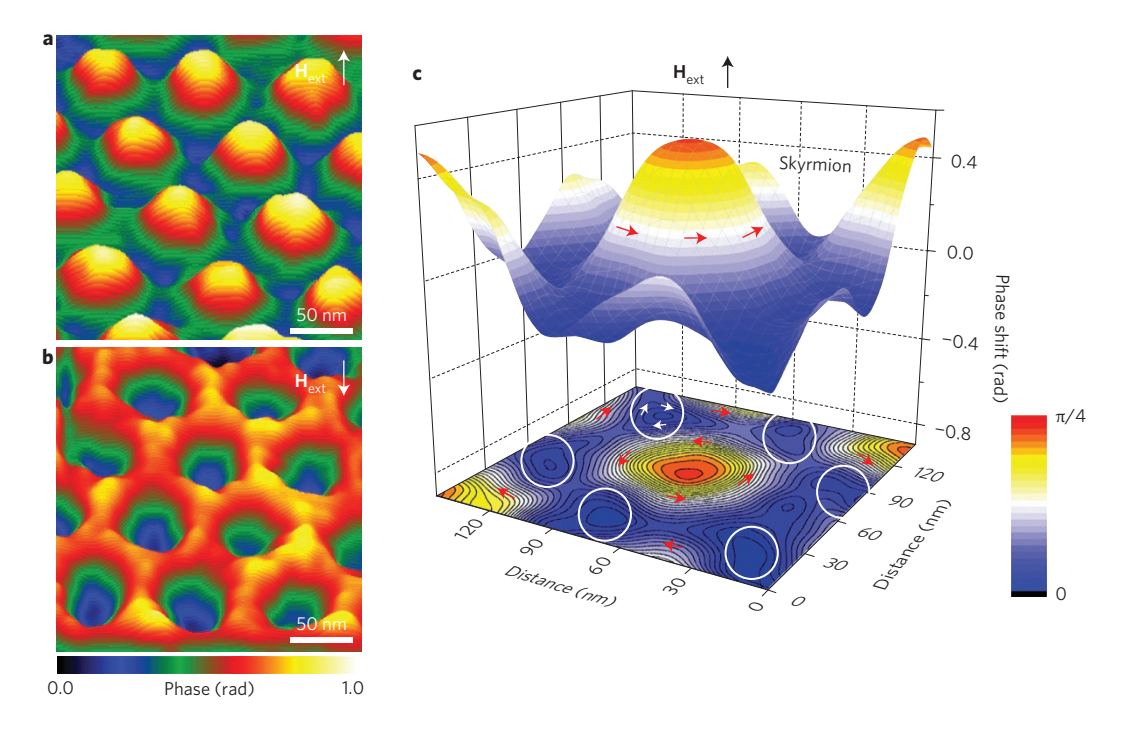


Figure 4 | Handedness reversal of magnetic flux flow with change in direction of the applied field. a,b, Surface plots of the phase image. The direction of applied field H_{ext} is indicated in each image. The sign reversal of the phase shift with change in applied field direction is clearly visible. c, Enlarged surface plot in the vicinity of a skyrmion. Red and white arrows represent the directions of lines of magnetic flux. Phase shift minima are observed in regions indicated by white circles.

to create interference between object waves illuminating a thin sample and reference waves passing through the vacuum. An artificial hole of diameter ~100 nm (indicated by the yellow circle in the figure) was created by the FIB technique to enable the phase images to be easily aligned for averaging. The phase image reconstructed from the hologram (Fig. 2b) shows a skyrmion lattice. The phase shifts of the electrons were affected by the superimposed electric and magnetic vector potentials, as given by equation (1). The phase shifts due to these potentials are hereafter referred to as $\varphi_{\rm E}$ and $\varphi_{\rm M}$, respectively. For precise phase measurement of weak phase objects such as skyrmions, φ_{M} and φ_{E} must be separated so that specimen roughness and other unwanted factors can be eliminated. The phase image in Fig. 2b shows $arphi_{
m E}$ – $arphi_{
m M}$ below the Curie transition temperature T_c , whereas Fig. 2c shows only $\varphi_{\rm E}$ because only the paramagnetic state is present above T_c. Simple subtraction of these two phase images (Fig. 2b,c) results in $\varphi_{\rm M}$ only, as shown in Fig. 3a, in which the difference between the equi-phase lines (white lines) corresponds to 0.1 rad. Note that the T_c of the thin samples in the present study was estimated to be ~35 K in both the 300 kV and 1,000 kV microscopes, which is 8 K lower than that of bulk $Fe_{0.5}Co_{0.5}Si$. The decrease in T_c was also observed in helimagnet MnSi thin samples in our previous report8.

A two-dimensional magnetic flux map of the skyrmion lattice is presented in the reconstructed phase image (Fig. 3b) and is represented by $\cos\varphi(x,y)$. In Fig. 3b, the black and white contour lines represent the lines of magnetic flux projected in the electron beam direction. The red arrows in Fig. 3c (enlarged image of the red square in Fig. 3b) indicate the direction of the in-plane component of the magnetic flux. An anticlockwise magnetic flux flow was observed in each skyrmion. In Fig. 3b,c, the phase difference between two black contour lines corresponds to $\Delta\varphi_{\rm M}=\pi/25$. From this phase difference, we can directly measure the normal in-plane component of the magnetic flux density (in the y direction), $B_{\rm n}(x,y)$, integrated through the specimen thickness. From

equation (1), after subtraction of two phase images (in Fig. 2b,c), the x gradient of phase $\Delta \varphi_{\rm M}(x,y)$ is given by

$$\frac{\partial \Delta \varphi_{\rm M}(x,y)}{\partial x} = -\frac{2\pi e}{h} B_{\rm n}(x,y) t(x,y) \tag{2}$$

where h/e is twice the flux quantum (4.1 × 10⁻¹⁵ Wb). For example, given the measured thickness (290 nm), we estimated the phase shift in the region of the asterisk in Fig. 3c to be 0.0174 rad nm⁻¹. Using equation (2), we determined the in-plane component of the magnetic flux density at this region to be 0.04 ± 0.005 T. Note that the magnetic flux observed here does not directly represent the emergent flux itself arising from the skyrmion topological charge.

The line profile for line A–B in Fig. 3a is plotted in Fig. 3d. It was fitted with a sinusoidal waveform (red curve), where the period of the skyrmion lattice was 120.8 ± 0.2 nm, in accordance with the helical period multiplied by $2/\sqrt{3}$ (refs 28,29). The observation that the φ integrated through the specimen thickness changes as a sinusoidal waveform indicates that spins rotate by 360° with a constant angle between the period of the skyrmion lattice in Fig. 3d. Further electron holographic observations with atomic resolution (towards achieving atomic column-by-column magnetic imaging) will be essential for local measurement of the Dzyalosinsky–Moriya (DM) interaction, as well as for an assessment of its role in determining the spin topography.

The handedness of the magnetic flux flow in a skyrmion lattice depends on the direction of the applied field. When the field was applied in one direction, the phase shift distribution exhibited bulging, as shown in Fig. 4a. When the field was applied in the opposite direction, bulging occurred in the opposite direction (Fig. 4b). This means that the handedness switched from anticlockwise to clockwise. Note that the φ show minima in the centre regions of a triangular skyrmion crystal. The handedness of the magnetic flux flow in these regions is believed to be opposite that

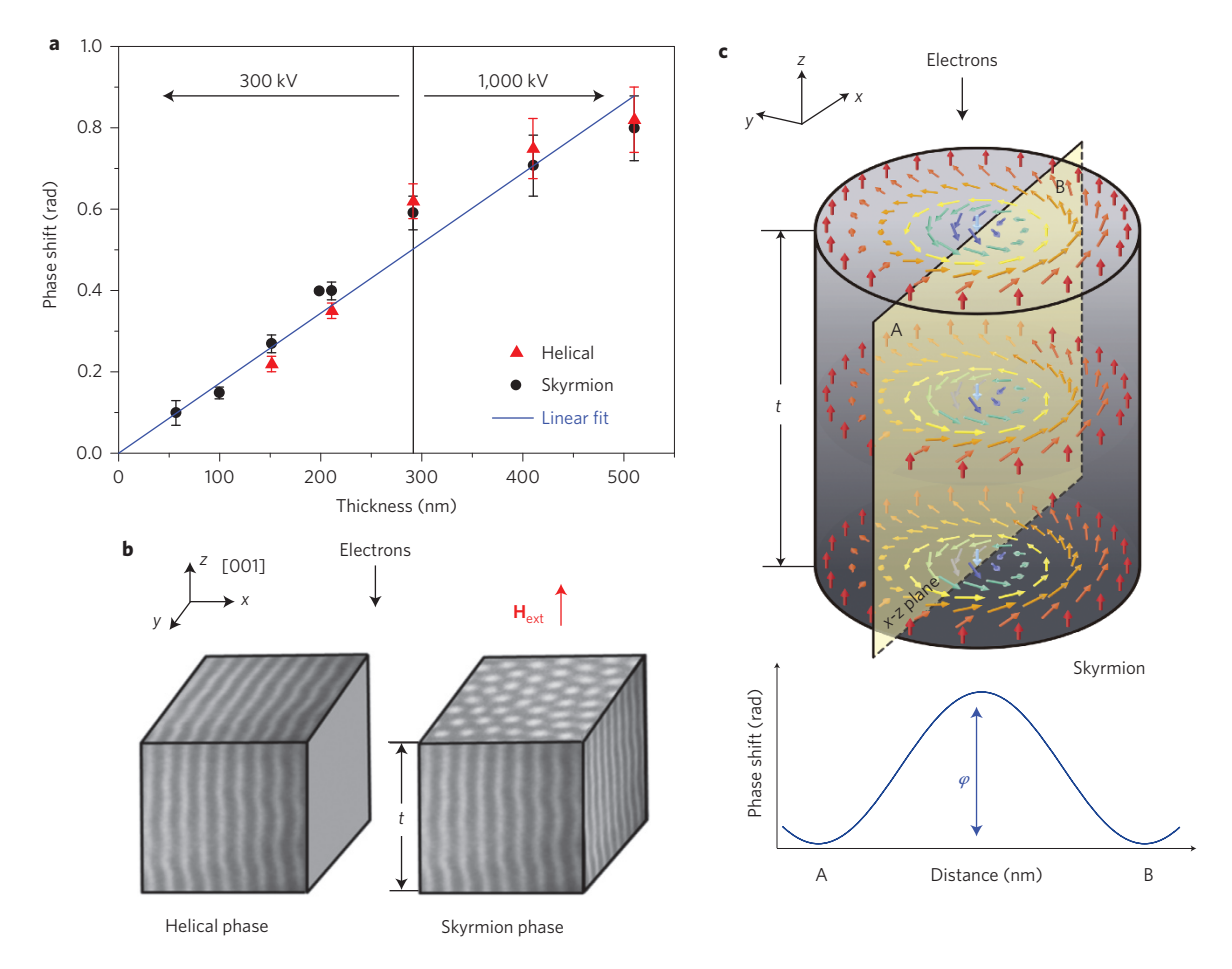


Figure 5 | Three-dimensional structures of skyrmions. a, Electron phase shifts of the helix and skyrmion as a function of sample thickness. Note that six samples were used for phase measurements (carried out using 300 and 1,000 kV microscopes). The slope of the linear fit line is 0.00173 rad nm⁻¹. Error bars represent the standard deviation. **b**, Schematic illustration of the three-dimensional structures of a helix and skyrmion. The black arrow indicates the direction of the incident electron beam and the red arrow that of the applied field. **c**, Schematic illustration showing the three-dimensional spin structure of a skyrmion and its phase shift profile for line A-B (in the x-z plane), integrated through specimen thickness t. Phase shifts φ were measured as the difference between the maxima and minima of the sinusoidal curve for line A-B in the x-z plane.

of a skyrmion, as indicated by the white circles and arrows in Fig. 4c. Although electron holography cannot detect magnetization parallel to the incident electron beams, it is reasonable to assume that the magnetic polarizations in two cores, one with minimum phase shift and one with maximum phase shift, are opposite each other, as previously reported⁶.

Next, we discuss the three-dimensional structures of helical and skyrmion phases in the direction of the z axis. The power of a 1,000 kV holography electron microscope is illustrated in Fig. 5a, which shows the thickness dependence of φ in a helix and in a skyrmion. Phase shifts φ were measured as the difference between the maxima and minima of the sinusoidal curve, as shown in Figs 3d and 5c. The phase shift (Fig. 5a) has a linear relationship with specimen thickness t, as shown by fitting using data measured for a skyrmion. The slope was found to be 0.00173 rad nm⁻¹. Furthermore, in Fig. 5a, the phase shift of a skyrmion can be seen to be quite similar to that of a helical phase. Depicted in Fig. 5c is a schematic illustration of the three-dimensional spin configuration in a skyrmion and its electron phase shift following the A-B line (in the x-z plane), integrated through t. Coloured arrows represent the magnetization direction at each point. It should be emphasized that, experimentally, the phase shift following the A-B line shows not only a sinusoidal curve fitting, but also a linear function with a stepped thickness from 55 nm to 510 nm, that is, $\varphi = 0.00173t$. From these electron holography results we concluded that the three-dimensional spin configuration of a skyrmion in the z direction is a cylinder, like in helimagnet ${\rm Fe_{0.5}Co_{0.5}Si}$, as illustrated in Fig. 5b,c.

In summary, the power of real-space imaging with precise phase measurements has enabled the visualization and quantification of the magnetic flux in a skyrmion lattice in Fe_{0.5}Co_{0.5}Si thin samples. The handedness of the magnetic flux flow of the skyrmions reversed direction when the field was applied in the opposite direction. Direct measurement of the electron phase shift in a helix and a skyrmion by using samples with stepped thicknesses revealed a linear relationship between the thickness and the phase shift (slope of 0.00173 rad nm⁻¹). Electron holography results can thus provide insight into the three-dimensional spin structures of a skyrmion lattice in helimagnet Fe_{0.5}Co_{0.5}Si. Our study demonstrates the potential of using a high-voltage holography electron microscope in various applications, such as the three-dimensional visualization magnetic fields in emergent matter systems spin-electronic devices.

Methods

The Fe $_{0.5}$ Co $_{0.5}$ Si single crystal (B20-type) was grown using the floating zone technique. Several thin samples with thicknesses from 55 nm to 510 nm were prepared using the FIB method (FB-2100, Hitachi) combined with a microsampling technique. The holography electron microscopes (HF-3300S, Hitachi) were used at acceleration voltages of 300 kV (electron wavelength of 1.969 pm) and 1,000 kV (0.872 pm), providing highly coherent waves and a bright electron source. High-

energy electron beams provided us with higher electron transmission capability, as well as a bright and coherent electron beam. Radiation damage to thin specimens. induced by incident electrons, is an important concern for data analysis. Once we saw a decrease in contrast (or phase shift) of a helix or skyrmion lattice during observations, which may have been due to radiation damage, we replaced this thin specimen with a new one. In our experiment, as shown in Fig. 1a, six thin specimens were used for electron holographic observations. For this reason, radiation damage effects were negligible. These microscopes have two positions at which the specimen can be located: the field-free position and the objective lens position. Electron holograms (with and without an applied field) were observed in the field-free position, at which the residual magnetic field was measured to be ~0.01 mT. A magnetic field (up to a maximum of 50 mT) was applied normal to the thin sample plane using a direction-free magnetic field application system³⁰. To record the holograms, a slow-scan charge-coupled-device (CCD) camera (UltraScan4000, Gatan) was used, with a pixel size of $4,096 \times 4,096$ (15 µm/pixel). To increase the phase resolution in the skyrmion lattice (Fig. 3), we averaged phase images reconstructed from 64 holograms taken consecutively under the same conditions. The exposure time for taking one hologram was 10 s. A double-tilt liquid-helium cooling holder (HLTDT, Gatan) was used to trigger a phase transition below the Curie transition temperature T_c . This enabled the specimen temperature to be reduced to ~5 K (the measured temperature was displayed on the cooling holder controller).

Received 23 August 2013; accepted 17 February 2014; published online 13 April 2014

References

- Fert, A., Cros, V. & Sampaio, J. Skyrmions on the track. Nature Nanotech. 8, 152–156 (2013).
- Iwasaki, J., Mochizuki, M. & Nagaosa, N. Universal current-velocity relation of skyrmion motion in chiral magnets. *Nature Commun.* 4, 1463 (2013).
- Rosch, A. Skyrmions: moving with the currents. Nature Nanotech. 8, 160–161 (2013).
- Pfleiderer, C. et al. Partial order in the non-Fermi-liquid phase of MnSi. Nature 427, 227–231 (2004).
- Muhlbauer, S. et al. Skyrmion lattice in a chiral magnet. Science 323, 915–919 (2009).
- Yu, X. Z. et al. Real-space observation of a two-dimensional skyrmion crystal. Nature 465, 901–904 (2010).
- Yu, X. Z. et al. Near room-temperature formation of a skyrmion crystal in thinfilms of the helimagnet FeGe. Nature Mater. 10, 106–109 (2011).
- Tonomura, A. et al. Real-space observation of skyrmion lattice in helimagnet MnSi thin samples. Nano Lett. 12, 1673–1677 (2012).
 Hairra S. et al. Sportaneous etomic scale menutic skyrmion lettice in two.
- 9. Heinze, S. *et al.* Spontaneous atomic-scale magnetic skyrmion lattice in two dimensions. *Nature Phys.* **7**, 713–718 (2011).
- 10. Milde, P. $\it{et~al.}$ Unwinding of a skyrmion lattice by magnetic monopoles. $\it{Science}$ 340, 1076–1080 (2013).
- Romming, N. et al. Writing and deleting single magnetic skyrmions. Science 341, 636–639 (2013).
- 12. Nagaosa, N., Yu, X. Z. & Tokura, Y. Gauge fields in real and momentum spaces in magnets: monopoles and skyrmions. *Phil. Trans. R. Soc. A* **370**, 5806–5819 (2012).
- Jonietz, F. et al. Spin transfer torques in MnSi at ultralow current densities. Science 330, 1648–1651 (2010).
- 14. Yu, X. Z. et al. Skyrmion flow near room temperature in an ultralow current density. Nature Commun. 3, 1–6 (2012).

- Lee, M., Kang, W., Onose, Y., Tokura, Y. & Ong, N. P. Unusual Hall effect anomaly in MnSi under pressure. Phys. Rev. Lett. 102, 186601 (2009).
- Neubauer, A. et al. Topological Hall effect in the A phase of MnSi. Phys. Rev. Lett. 102, 186602 (2009).
- 17. Binz, B. & Vishwanath, A. Theory of helical spin crystals: phases, textures, and properties. *Phys. Rev. B* **74**, 214408 (2006).
- Park, J. H. & Han, J. H. Zero-temperature phases for chiral magnets in three dimensions. *Phys. Rev. B* 83, 184406 (2011).
- 19. Kanazawa, N. *et al.* Possible skyrmion-lattice ground state in the B20 chiral-lattice magnet MnGe as seen via small-angle neutron scattering. *Phys. Rev. B* **86.** 134425 (2012).
- Seki, S., Yu, X. Z., Ishiwata, S. & Tokura, Y. Observation of skyrmions in a multiferroic material. Science 336, 198–201 (2012).
- 21. Tonomura, A. et al. Motion of vortices in superconductors. Nature 397, 308–309 (1999).
- 22. Park, H. S. et al. Direct observation of magnetization reversal in thin $Nd_2Fe_{14}B$ film. J. Appl. Phys. **97**, 033908 (2005).
- Junginger, F. et al. Spin torque and heating effects in current-induced domain wall motion probed by transmission electron microscopy. Appl. Phys. Lett. 90, 132506 (2007).
- Park, H. S., Baskin, J. S. & Zewail, A. H. 4D Lorentz electron microscopy imaging: magnetic domain wall nucleation, reversal, and wave velocity. *Nano Lett.* 10, 3796–3803 (2010).
- 25. Tonomura, A. Electron Holography 2nd edn (Springer-Verlag, 1999).
- Cowley, J. M. & Spence, J. C. H. Principles and Theory of Electron Holography, Introduction to Electron Holography (eds Volkl, E., Allard, L. F. & Joy, D. C.) (Kluwer Academic/Plenum, 1998).
- Park, H. S. et al. Nanoscale magnetic characterization of tunneling magnetoresistance spin valve head by electron holography. Small 8, 3640–3646 (2012).
- Shibata, K. et al. Towards control of the size and helicity of skyrmions in helimagnetic alloys by spin-orbit coupling. Nature Nanotech. 8, 723–728 (2013).
- Nagaosa, N. & Tokura, Y. Topological properties and dynamics of magnetic skyrmions, *Nature Nanotech.* 8, 899–911 (2013).
- Harada, K., Endo, J., Osakabe, N. & Tonomura, A. Direction-free magnetic field application system. J. Surf. Sci. Nanotech. 6, 29–34 (2008).

Acknowledgements

The authors thank Y.A. Ono for critical reading of the manuscript. This research was supported by a grant from the Japan Society for the Promotion of Science (JSPS) through the 'Funding Program for World-Leading Innovative R&D on Science and Technology (FIRST Program)', initiated by the Council for Science and Technology Policy (CSTP) under the programmes 'Development and Application of an Atomic-resolution Holography Electron Microscope' and 'Quantum Science on Strong Correlation'.

Author contributions

H.S.P., A.T. and Y.T. conceived and designed the experiments. H.S.P., S.A., T.T., T.A. and T.M. performed the experiments and analysed the data. N.K. and Y.O. contributed to the synthesis of samples. H.S.P. and Y.T. wrote the paper. All authors discussed the results and commented on the manuscript.

Additional information

Reprints and permissions information is available online at www.nature.com/reprints. Correspondence and requests for materials should be addressed to H.S.P.

Competing financial interests

The authors declare no competing financial interests.